Supporting Information for

Effective Surface Treatment for High-Performance Inverted $CsPbI_2Br$ Perovskite Solar Cells with Efficiency of 15.92%

Sheng Fu[1, 2], Xiaodong Li[3], Li Wan[1], Wenxiao Zhang[1, 2], Weijie Song[1, 2], Junfeng Fang[1, 2, 3, *]

[1]Ningbo Institute of Materials Technology and Engineering, Chinese Academy of Sciences, Ningbo 315201, People's Republic of China

[2]Center of Materials Science and Optoelectronics Engineering, University of Chinese Academy of Sciences, Beijing 100049, People's Republic of China

[3]School of Physics and Electronics Science, Engineering Research Center of Nanophotonics & Advanced Instrument, Ministry of Education, East China Normal University, Shanghai 200241, People's Republic of China

*Corresponding author. E-mail: jffang@phy.ecnu.edu.cn (Junfeng Fang)

Supplementary Table and Figures

Table S1 A summary of $CsPbI_2Br$-based inorganic perovskite solar cells researches with the detail performance parameters and stability

Devices structure	V_{oc} (V)	PCE (%)	Stability	Refs.
ITO/PEDOT:PSS/$CsPbI_2Br$/PCBM/BCP/Al	1.06	6.8	non*	[S1]
FTO/NiMgLiO/ $CsPbI_2Br$ /PCBM/BCP/Ag	0.98	9.14	L* 90% for 500	[S2]
ITO/NiOx/$CsPbI_2Br$ /C60/BCP/Ag	1.05	10.4	non	[S3]
FTO/NiO/$CsPbI_2Br$/ZnO/C60/Ag	1.14	13.30	T* 85% for 360 h	[S4]
FTO/NiO/$CsPbI_2Br$:In/ZnO/C60/Ag	1.15	13.74	M* 100% for 100 h	[S5]
FTO/NiMgLiO/$CsPbI_2Br$/TiO_2/Ag	1.26	14.00	T* 92.1% for 1000 h	[S6]
ITO/NiOx/$CsPbI_2Br$/Nb_2O_5/Ag	1.20	14.11	S* 98% for 30 d	[S7]
FTO/NiMgLiO/$CsPbI_2Br$/TiO_2/Sb	1.28	14.8	L 90% for 1000 h	[S8]
ITO/P3CT/$CsPbI_2Br$:Ni/PCBM/C60/BCP/Ag	1.141	13.88	L 60% for 500 h	[S9]
FTO/NiO/$CsPbI_2Br$/ZnO/C60+TPFPB+$LiClO_4$/ Ag	1.23	15.19	S 91.8% for 72 d	[S10]
ITO/TPE-S/$CsPbI_2Br$/PCBM/ZnO/Ag	1.26	15.4	L 84% for 400 h	[S11]
ITO/P3CT-N/$CsPbI_2Br$:FABr /PCBM/C60/BCP/Ag	1.223	15.92	M 91.7% for 1300 h; L 81.8% for 500 h; T 93.6% for 36 d	Our

ITO/SnO_2/$CsPbI_2Br$/Spiro/Au	1.22	14.21	non	[S12]
FTO/TiO_2/$CsPbI_2Br$:Mn/QDs/PTAA/Au	1.172	14.09	M* 97% for 840 h	[S13]
FTO/TiO_2/$CsPbI_2Br$:Zn/Spiro/Ag	1.18	13.60	M 85% for 480 h	[S14]
ITO/TiO_2/$CsPbI_2Br$:Cu/Spiro/MoO_3/Ag	1.19	16.15	M 95% for 720 h	[S15]
FTO/TiO_2/$CsPbI_2Br$/QDs/PTAA/Au	1.22	14.81	M 100% for 720 h	[S16]
ITO/SnO_2/ZnO/$CsPbI_2Br$/Spiro/MoO_3/Ag	1.23	14.6	non	[S17]
ITO/TiO_2/$CsPbI_2Br$/Spiro/Au	1.23	16.07	M 95% for1000 h	[S18]
ITO/SnO_2/PN4N/$CsPbI_2Br$/PDCBT/MoO_3/Ag	1.30	16.2	L* 90% for 400 h	[S19]
FTO/TiO_2/$CsPbI_2Br$:Ac/Spiro/Au	1.30	15.56	M 86% for 336 h	[S20]
ITO/SnO_2/$CsPbI_2Br$/$CsPbI_xBr_y$/Spiro/Au	1.32	15.50	T 80% for 350 h	[S21]
ITO/SnO_2/ZnO/$CsPbI_2Br$/PSQ2/MoO_3/Ag	1.27	15.50	L 83% for 300 h	[S22]
ITO/SnO_2/$CsPbI_2Br$:CsBr/Spiro/Au	1.271	16.37	S 86% for 1368 h	[S23]
ITO/TiO_2/$CsPbI_2Br$/Spiro/Au	1.12	14.69	M 70% for 20 h	[S24]
FTO/TiO_2/$CsPbI_2Br$:Eu/Spiro/Au	1.22	13.34	L 93% for 370 h	[S25]
FTO/TiO_2/$CsPbI_2Br$ /QDs:FAI/PTAA/Au	1.223	14.12	M 100% for 30 d	[S26]
ITO/ZnO:Cs/$CsPbI_2Br$/Spiro/MoO_3/Ag	1.28	16.34	M 96% for 200 h; T 81% for 200 h	[S27]
ITO/SnO_2/$CsPbI_2Br$:O/Spiro/Au	1.18	15.17	M 92.3% for 32 d	[S28]
ITO/TiO_2/$CsPbI_2Br$ /Spiro/PTAA/Ag	1.23	16.58	T 90% for 500 h; M 90% for 4000 h; L 90% for 1000 h	[S29]
ITO/SnO_2/$CsPbI_2Br$/Spiro/Au	1.286	15.58	M 83.4% for 1540 h; L100% for 350 h	[S30]
ITO/TiO_2/$CsPbI_2Br$ /Spiro/Au	1.32	16.79	M 90% for 1000 h;	[S31]

* T is the thermal stability, M is the moisture stability, S is the storage stability at N_2 atmosphere and L is the operational stability. A, A and A present the inverted structure $CsPbI_2Br$ devices, this work and the regular structure $CsPbI_2Br$ devices.

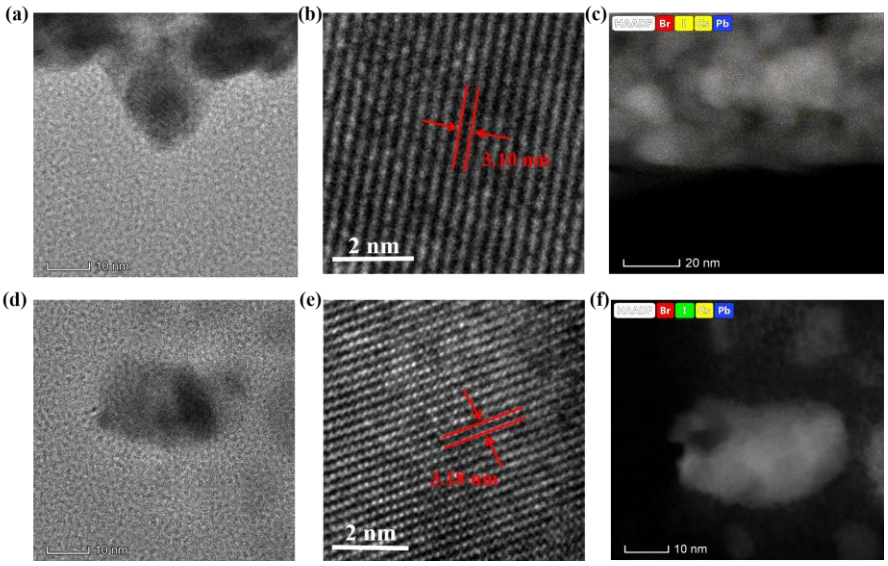

Fig. S1 TEM images of the Ref and 8F $CsPbI_2Br$ films. (**a-c**) TEM images and EDX

element mapping of Ref. (**b-d**) The TEM images and EDX element mapping of 8F $CsPbI_2Br$. The treated films show an enlarged lattice space, which indicates the incorporation of FA^+. From the EDX mapping, the Ref shows a Br/I ratio of 48.58% while treated films present a ratio of 56.43%, which prove the Br-rich.

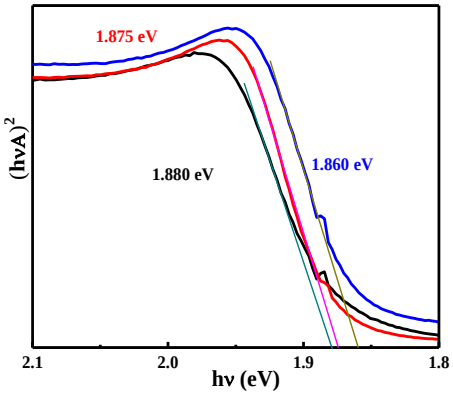

Fig. S2 Kubelka-Munk spectra of the corresponding films based on the absorption spectrum

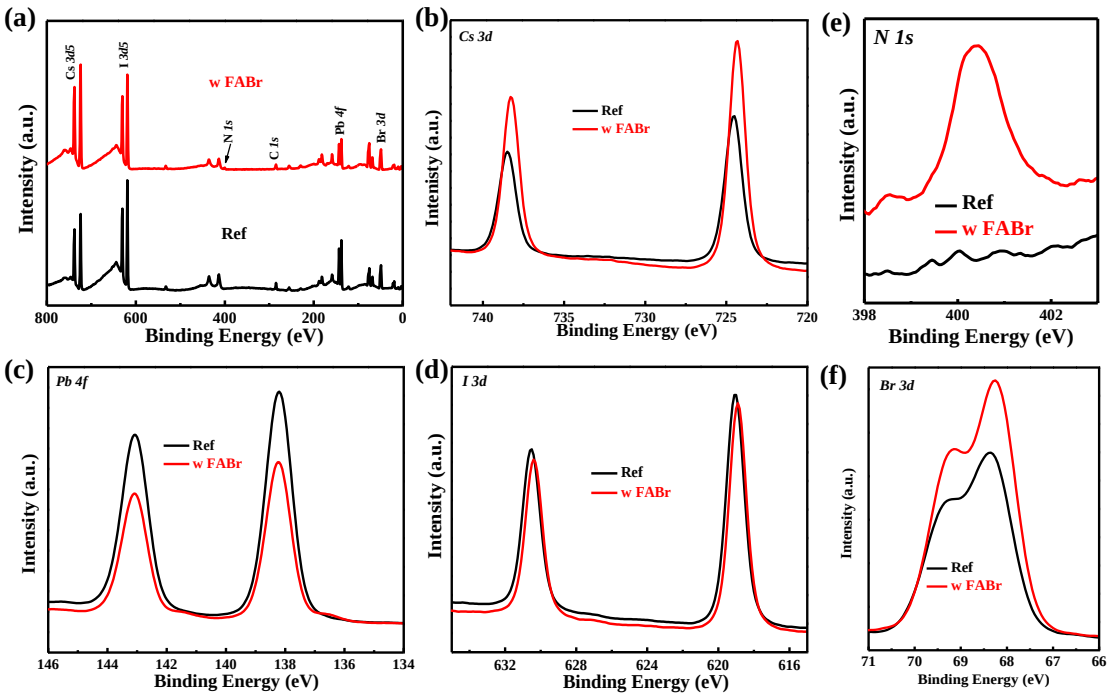

	Cs	Pb	I	Br	N
Atomic (%)	16.97	9.61	23.24	15.23	0.1
Atomic (%)	25.6	6.65	21.62	20.06	2.19

Fig. S3 The XPS spectrum of Ref and 8F $CsPbI_2Br$ films. (**a**) Full XPS spectra. (**b**) Cs 3d, (**c**) Pb 4f, (**d**) I 3d (**e**) N 1s and (**f**) Br 3d core-level spectra and the quantitative XPS results

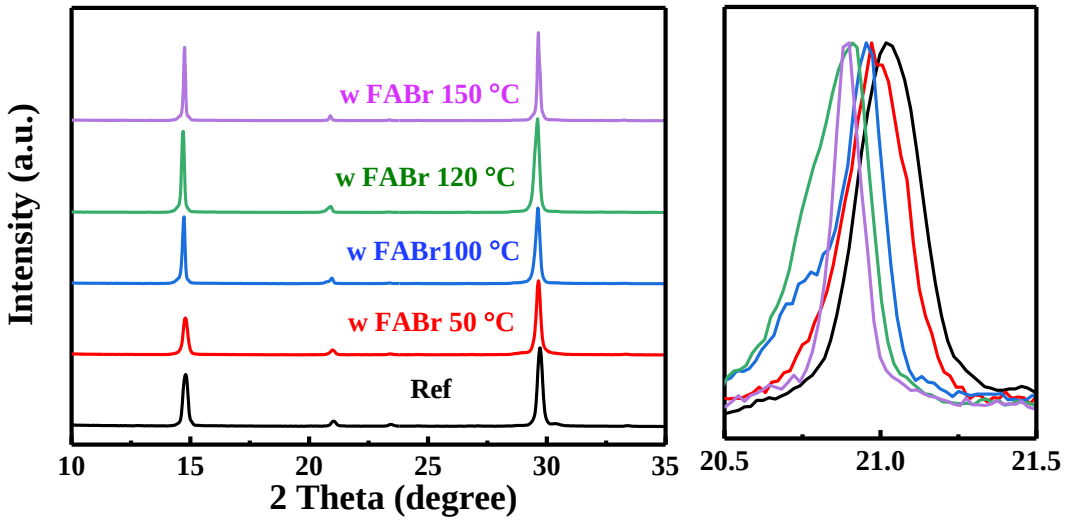

Fig. S4 XRD patterns of the FABr treating films annealed at various temperature

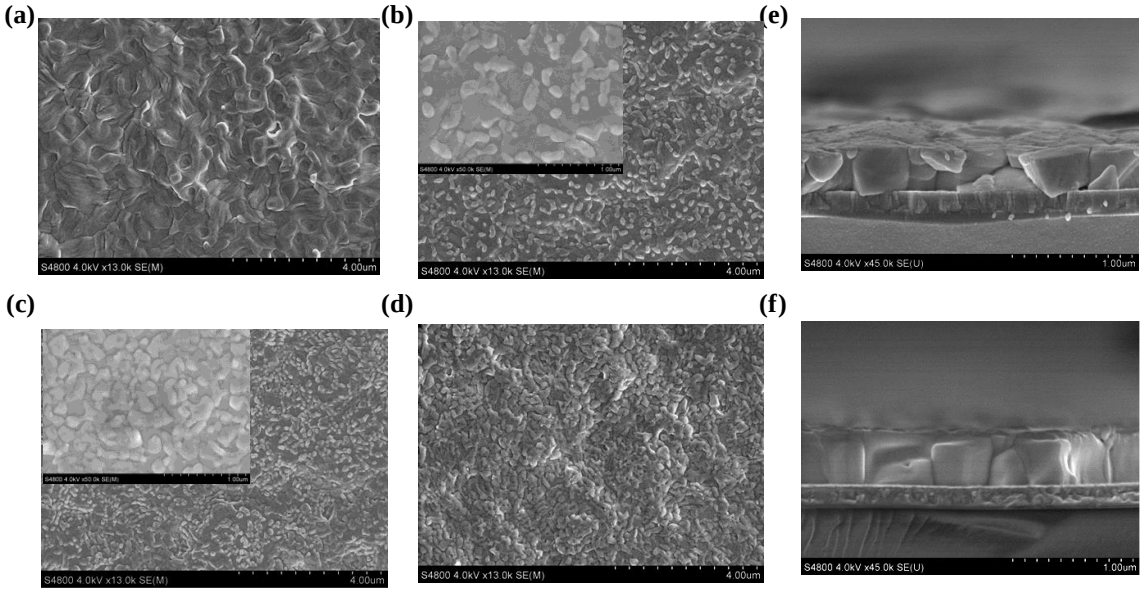

Fig. S5 Top-view SEM images of (**a**) the Ref, (**b**) 4, (**c**) 6, and (**d**) 8 mg mL^{-1} FABr. The cross-sectional SEM images of (**e**) the Ref and (**f**) the 8 mg mL^{-1} FABr films. With the FABr treated concentration increase, the covered region by AX gradually distribute from the GBs toward full surface and almost covered with 8 mg mL^{-1}. Also, the cross-sectional SEM image of treated film reveals a thin consequent covered layer compared with the Ref and the thickness of perovskite is about 500 nm.

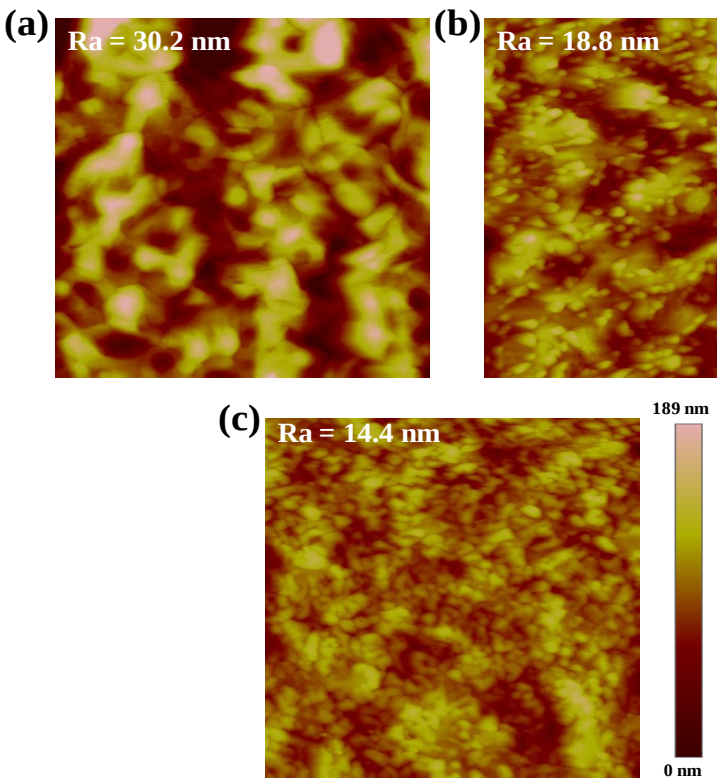

Fig. S6 AFM images of (**a**) Ref, (**b**) 4F $CsPbI_2Br$ and (**c**) 8F $CsPbI_2Br$ films. The area is 5×5 μm. The modified films show reduced surface roughness, which indicates the better contact with the ETL

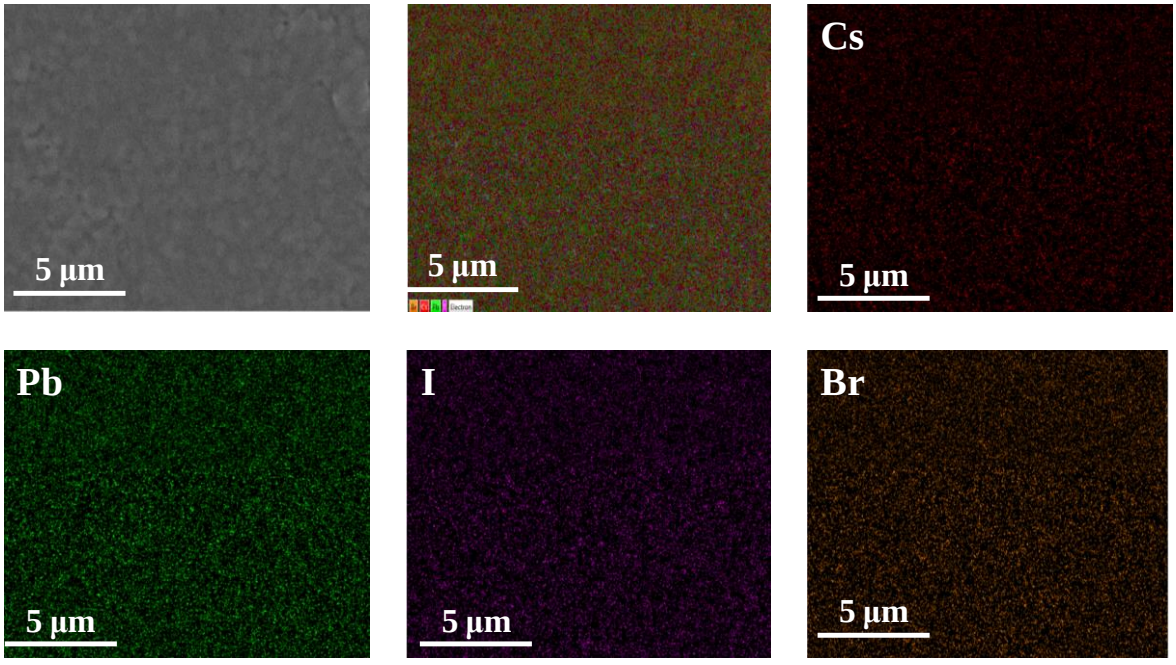

Fig. S7 The EDX top-view element mapping of Ref film. The element ratio reveals 20.58% of Cs element, 20.12% of Pb element, 40.14% of I element and 19.26% of Br, which consists with the Stoichiometric ratio of $CsPbI_2Br$

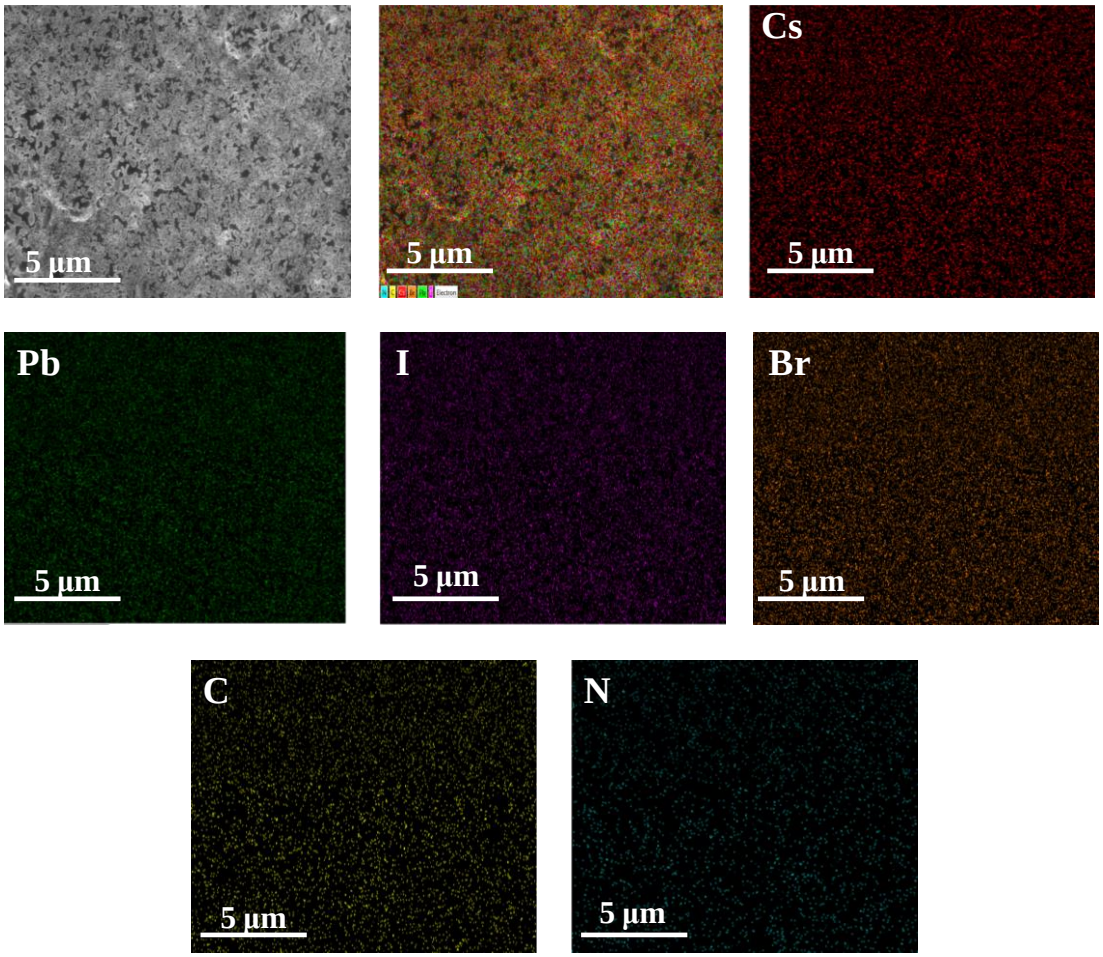

Fig. S8 EDX top-view element mapping of the 8 mg mL^{-1} FABr treated film. The film reveals the element ratio of 14.75% for C element, 2.08% for N element, 19.40% for Cs element, 14.16% for Pb element, 28.56% for I element and 21.05% for Br element. Associated the changed morphology and the component at surface, it could infer that the covered layer (AX) consists of FA/Cs and Br/I

Table S2 TRPL fitting results of the various treated films on the glass substrate

Sample	τ_1 (ns)	A_1	τ_2 (ns)	A_2	τ_{avg} (ns)*
Ref	3.88	0.27	16.57	0.73	15.56
4 FABr	3.12	0.24	12.84	0.76	12.15
8 FABr	0.75	0.34	7.48	0.66	7.15
4 EABr	4.24	0.12	22.98	0.88	22.52
2 PABr	10.56	0.14	25.24	0.86	24.30
6 MABr	2.65	0.22	9.65	0.78	9.15

* The τ_{avg} is calculated with the formal : $\tau_{avg}= (A_1\tau_1^2+ A_2\tau_2^2)/(A_1\tau_1+ A_2\tau_2)$ [S11].

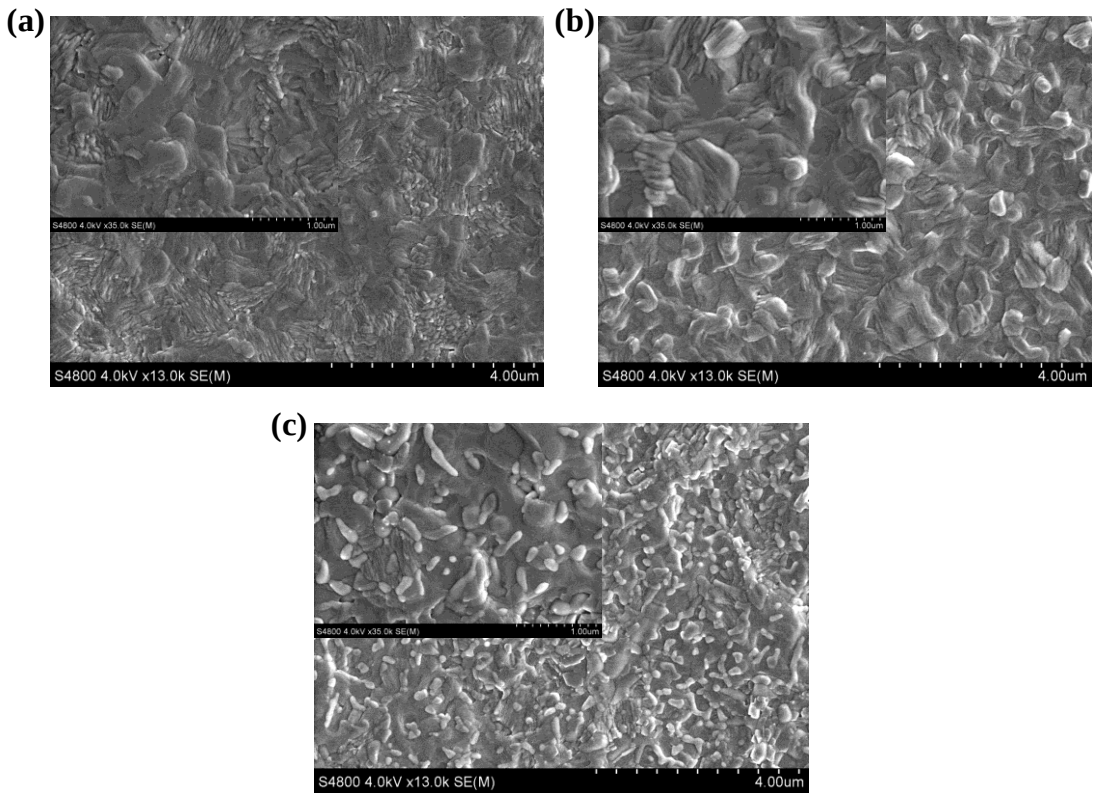

Fig. S9 Top-view SEM images of (**a**) 4 mg mL^{-1} EABr, (**b**) 2 mg mL^{-1} PABr and (**c**) 6 mg mL^{-1} MABr treated $CsPbI_2Br$ films. The inset images are the enlarged morphology of related films. Comparing to EABr and PABr treatment, MABr treated films exhibits the similar morphology with the second phase covering the surface.

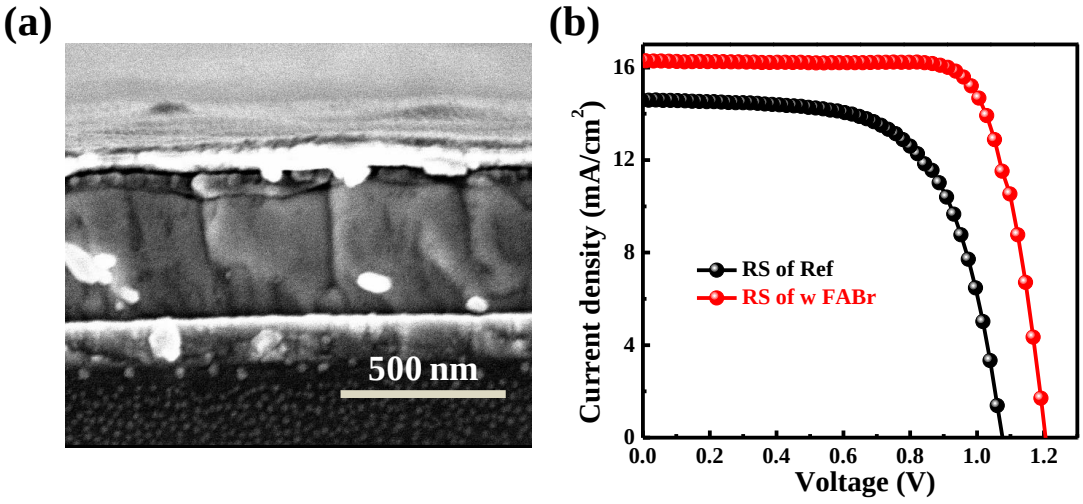

Fig. S10 (**a**) The cross-sectional SEM image of the inverted $CsPbI_2Br$ device with a structure of ITO/P3CT-N/$CsPbI_2Br$/PCBM/C60/BCP/Ag. The Ag electrode is deposited about 80 nm for convenient sample preparation. (**b**) The reverse scanning *J-V* curves of the champion devices of Ref and 8F treatment

Table S3 Photovoltaic parameters of the reverse scanning *J-V* curves

Sample	V_{oc} (V)	J_{sc} (Ma cm^{-2})	FF (%)	PCE (%)
Ref	1.075	14.60	64.26	10.08
8F $CsPbI_2Br$	1.201	16.03	76.24	14.97

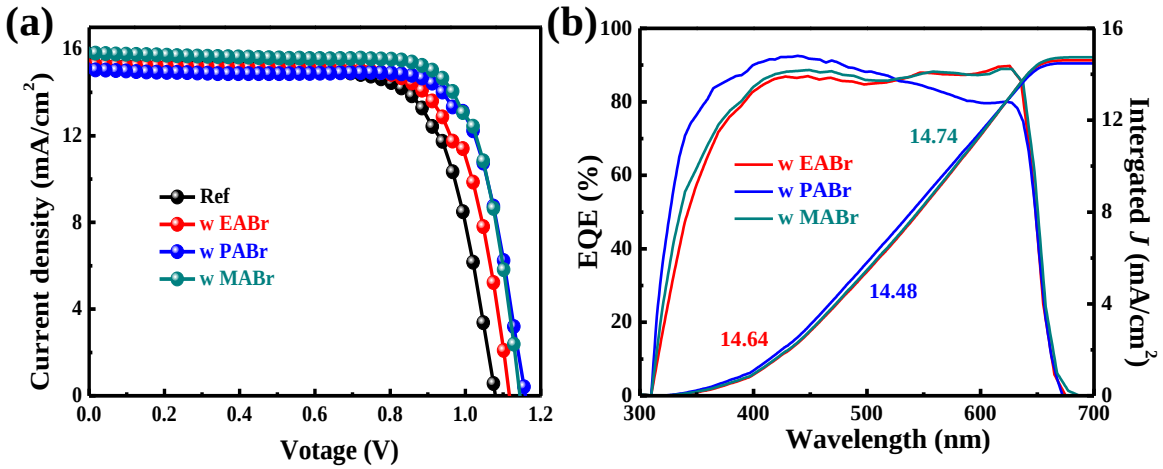

Fig. S11 J-V curves (**a**) and EQE spectra (**b**) of champion devices with 4 mg mL^{-1} EABr, 2 mg mL^{-1} PABr, and 6 mg mL^{-1} MABr treated

Table S4 The photovoltaic parameters of the *J-V* curves for EABr, PABr and MABr treated devices

Sample	V_{oc} (V)	J_{sc} (mA cm^{-2})	FF (%)	PCE (%)
4 EABr	1.117	15.26	73.46	12.53
2 PABr	1.159	15.04	75.16	13.10
6 MABr	1.145	15.80	76.15	13.776

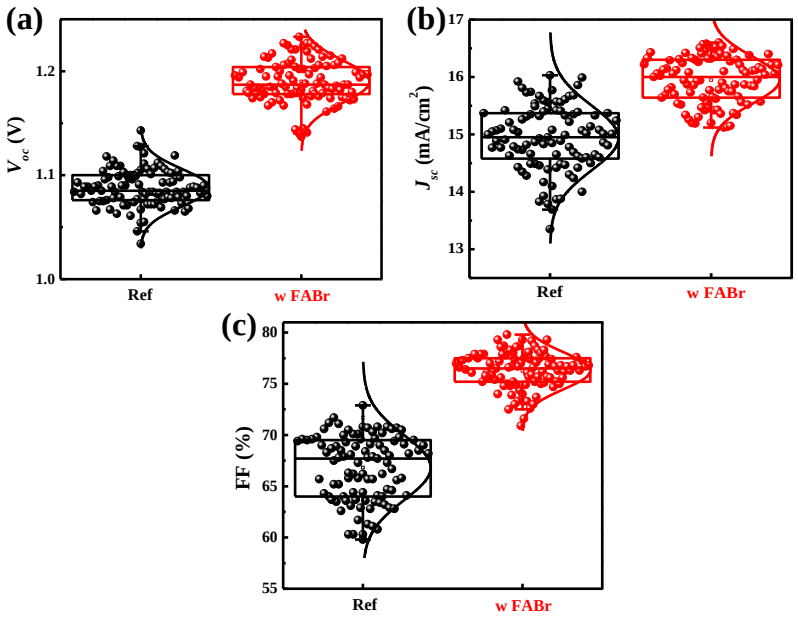

Fig. S12 Statistic spectrum of the parameter of the Ref and 8F treated devices. Statistics (**a**) Voc, (**b**) Jsc and (**c**) FF from 100 individual devices

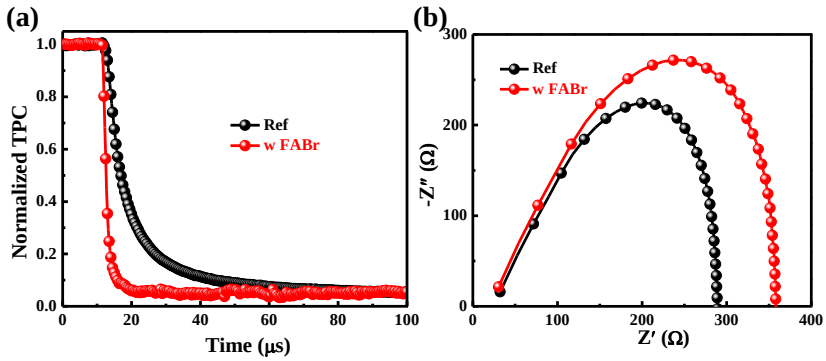

Fig. S13 (**a**) TPC spectra of the Ref device and 8F treated devices. In comparison with the Ref, the treated device shows a faster carrier transport, which benefits from the suppressed defects and induced gradient band structure. (**b**) Nyquist plots of of the Ref device and 8F treated devices. Benefiting from the effective passivation and promoted carrier transport, the 8F CsPbI2Br device reveals the larger R_{rec} than the Ref.

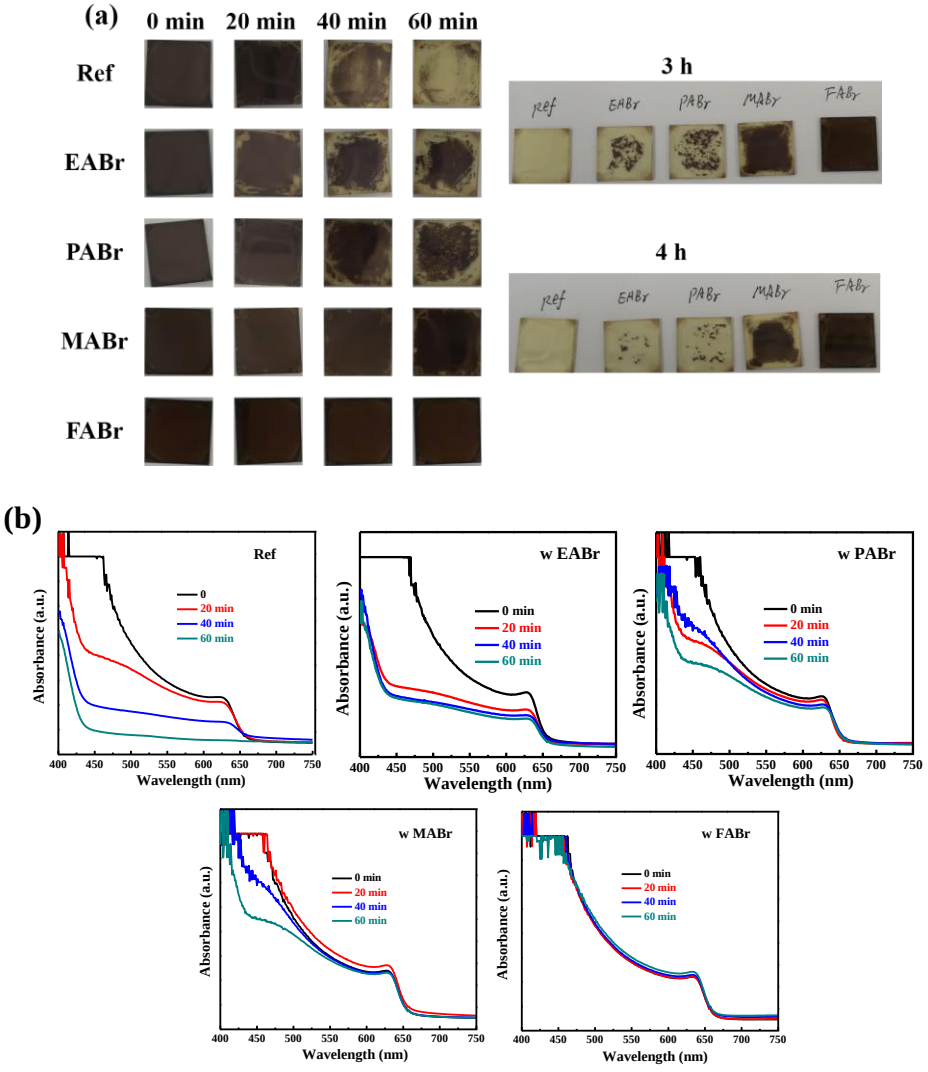

Fig. S14 Phase stability of films treated with various ABr after exposing to an

ambient environment with controlled RH 40%. (**a**) Photograph of various films VS aging time. (**b**) Related absorption spectra. Based on these comparisons, it can conclude that the FABr treated filmis gifted the most tolerance from moisture erosion.

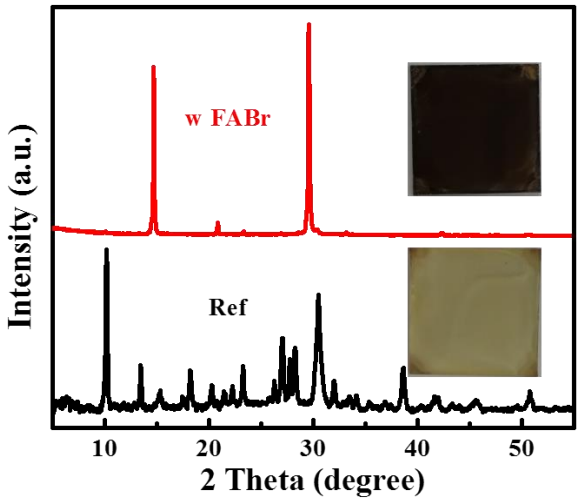

Fig. S15 XRD patterns and photograph of the Ref and 8F treated film after aging under RH 40% for 5 h. The 8F film remains α phase (black film) while the Ref have transmitted into γ phase (yellow color film)

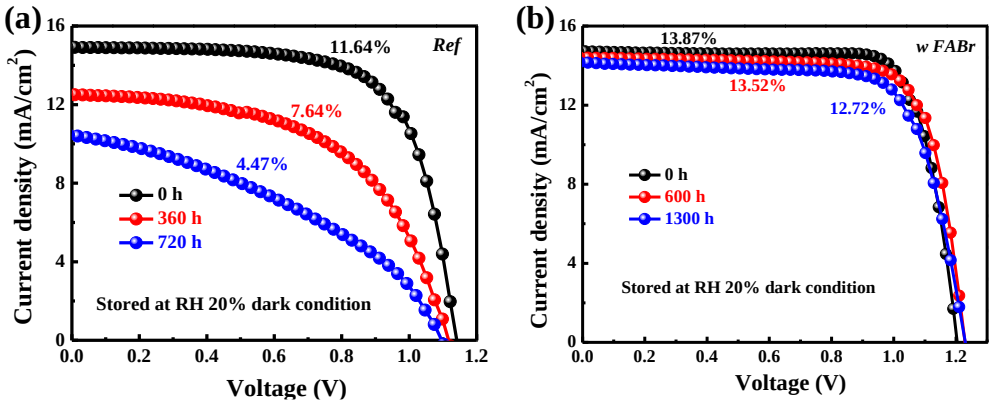

Fig. S16 *J-V* curves of the devices aged under RH 20%: (**a**) Ref and (**b**) 8F devices

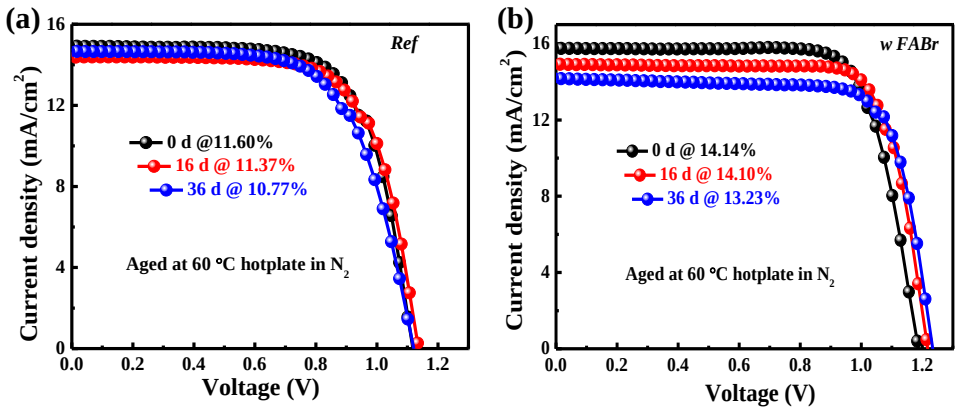

Fig. S17 *J-V* curves of the devices aged at 60 °C hotplate: (**a**) Ref and (**b**) 8F devices

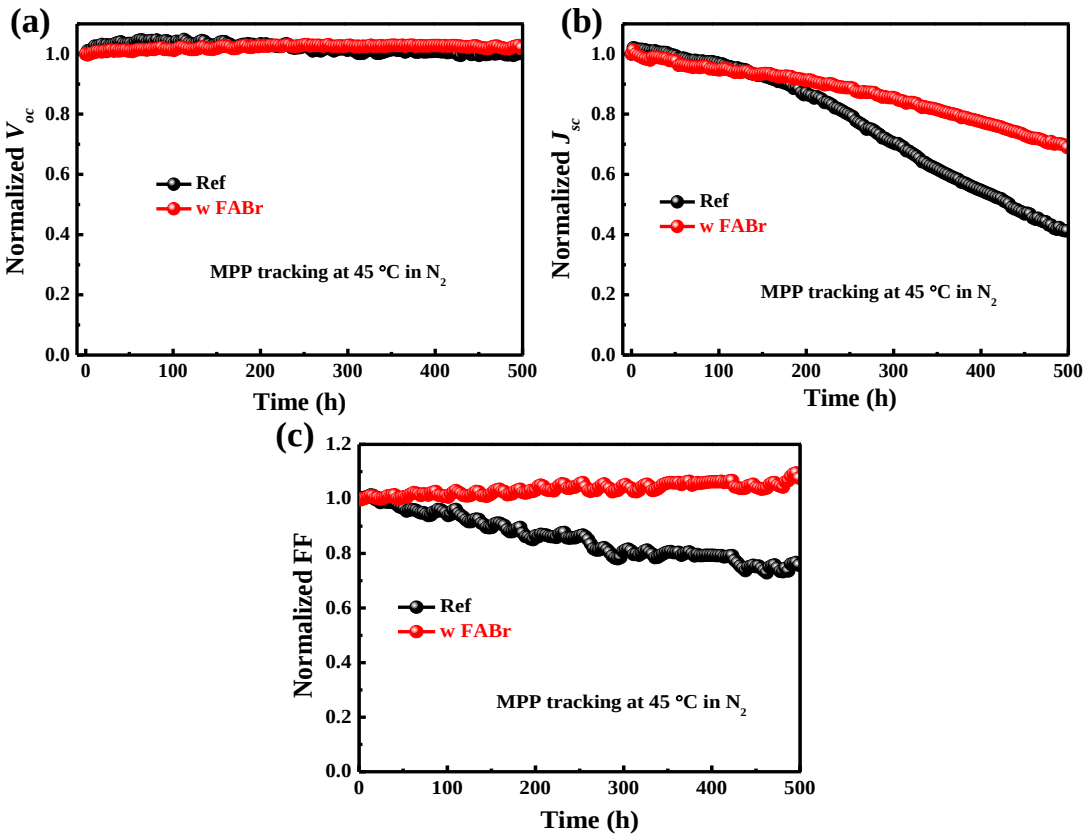

Fig. S18 Photovoltaic parameters changes under MPP tracking at 45 °C for 500 h

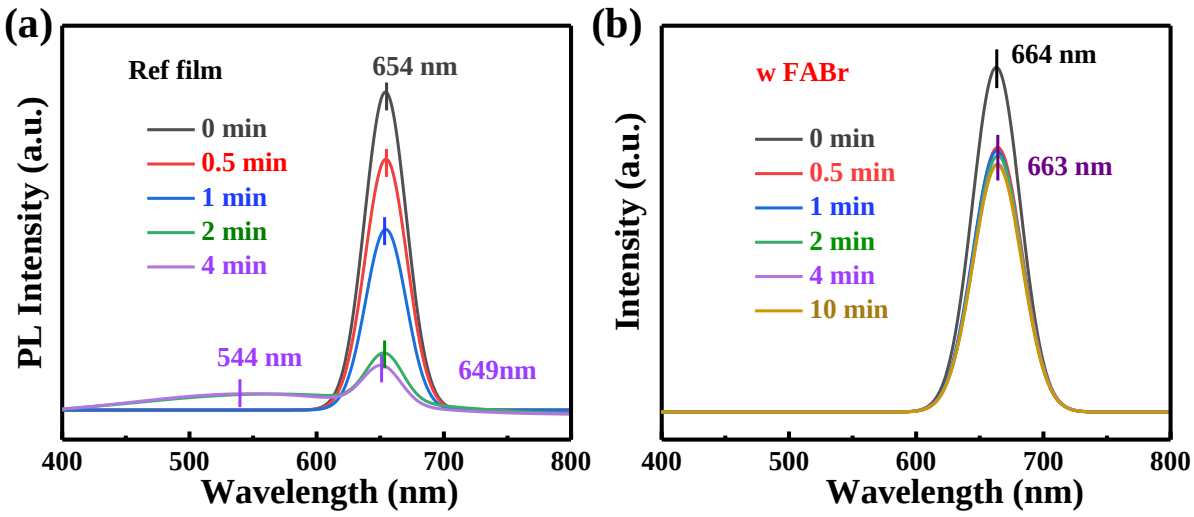

Fig. S19 PL spectra of the Ref (**a**) and FABr (**b**) modified films illuminated with the 193 nm UV laser with energy of 3 mJ in vacuum box. The Ref film reveals the serious phase separation while the treated film with good stability [S32].

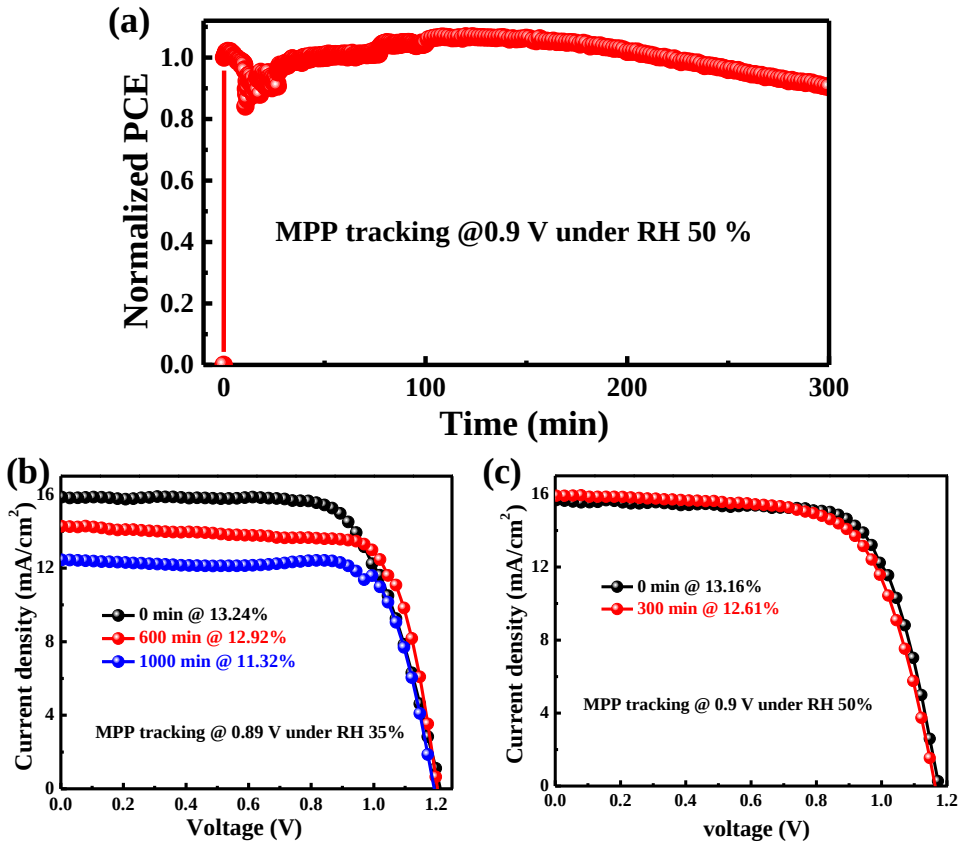

Fig. S20 MPP measurements under ambient condition. (**a**) MPP plots of the device under RH 50% for 300 min. (**b**) *J-V* curves of the device after MPP tracking under RH 35%. (**c**) J-V curves of the device after MPP measurement under RH 50% for 300 min

Supplementary References

[S1] R. E. Beal, D. J. Slotcavage, T. Leijtens, A. R. Bowring, R. A. Belisle et al., Cesium lead halide perovskites with improved stability for tandem solar Cells. J. Phys. Chem. Lett. **7,** 746 (2016). https://doi.org/10.1021/acs.jpclett.6b00002

[S2] S. Zhang, S. Wu, W. Chen, H. Zhu, Z. Xiong et al., Solvent engineering for efficient inverted perovskite solar cells based on inorganic $CsPbI_2Br$ light absorber. Mater. Today Energy **8**, 125 (2018). https://doi.org/10.1016/j.mtener.2018.03.006

[S3] H. Rao, S. Ye, F. Gu, Z. Zhao, Z. Liu, Z. Bian, C. Huang, Morphology controlling of all-inorganic perovskite at low temperature for efficient rigid and flexible solar cells. Adv. Energy Mater. **8**, 1800758 (2018). https://doi.org/10.1002/aenm.201800758

[S4] C. Liu, W. Li, C. Zhang, Y. Ma, J. Fan, Y. Mai, All-Inorganic $CsPbI_2Br$ perovskite solar cells with high efficiency exceeding 13%. J. Am. Chem. Soc.

140, 3825 (2018). https://doi.org/10.1021/jacs.7b13229

[S5] C. Liu, W. Li, H. Li, H. Wang, C. Zhang et al., Structurally reconstructed $CsPbI_2Br$ perovskite for highly stable and square-centimeter all-inorganic perovskite solar cells. Adv. Energy Mater. **9**, 1803572 (2019). https://doi.org/10.1002/aenm.201803572

[S6] S. Zhang, W. Chen, S. Wu, R. Chen, Y. Huang et al., A general strategy to prepare high-quality inorganic charge-transporting layers for efficient and stable all-layer-inorganic perovskite solar cells. J. Mater. Chem. A **7**, 18603 (2019). https://doi.org/10.1039/C9TA05802H

[S7] X. Liu, Y. Xiao, Q. Zeng, J. Jiang, Y. Li, Large-area organic-free perovskite solar cells with high thermal stability. J. Phys. Chem. Lett. **10**, 6382 (2019). https://doi.org/10.1021/acs.jpclett.9b02644

[S8] S. Zhang, W. Chen, S. Wu, R. Chen, Z. Liu et al., Hybrid inorganic electron-transporting layer coupled with a halogen-resistant electrode in $CsPbI_2Br$-based perovskite solar cells to achieve robust long-term stability. ACS Appl. Mater. Interfaces **11**, 43303 (2019). https://doi.org/10.1021/acsami.9b17464

[S9] L. Chen, L. Wan, X. Li, W. Zhang, S. Fu et al., Inverted all-inorganic $CsPbI_2Br$ perovskite solar cells with promoted efficiency and stability by nickel incorporation. Chem. Mater. **31**, 9032 (2019). https://doi.org/10.1021/acs.chemmater.9b03277

[S10] C. Liu, Y. Yang, C. Zhang, S. Wu, L. Wei et al., Tailoring C60 for efficient inorganic $CsPbI_2Br$ perovskite solar cells and modules. Adv. Mater. **32**, e1907361 (2020). https://doi.org/10.1002/adma.201907361

[S11] K. Jiang, J. Wang, F. Wu, Q. Xue, Q. Yao et al., Dopant-free organic hole-transporting material for efficient and stable inverted all-inorganic and hybrid perovskite solar cells. Adv. Mater. **32**, e1908011 (2020). https://doi.org/10.1002/adma.201908011

[S12] P. Wang, X. Zhang, Y. Zhou, Q. Jiang, Q. Ye et al., Solvent-controlled growth of inorganic perovskite films in dry environment for efficient and stable solar cells. Nat. Commun. **9**, 2225 (2018). https://doi.org/10.1038/s41467-018-04636-4

[S13] D. Bai, J. Zhang, Z. Jin, H. Bian, K. Wang et al., Interstitial Mn^{2+}-driven high-aspect-ratio grain growth for low-trap-density microcrystalline films for record efficiency $CsPbI_2Br$ solar cells. ACS Energy Lett. **3**, 970 (2018). https://doi.org/10.1021/acsenergylett.8b00270

[S14] H. Sun, J. Zhang, X. Gan, L. Yu, H. Yuan et al., Pb-reduced $CsPb_{0.9}Zn_{0.1}I_2Br$ thin films for efficient perovskite solar cells. Adv. Energy Mater. **9**, 1900896 (2019). https://doi.org/10.1002/aenm.201900896

[S15] K. L. Wang, R. Wang, Z. K. Wang, M. Li, Y. Zhang et al., Tailored phase transformation of $CsPbI_2Br$ films by copper(ii) bromide for high-performance all-inorganic perovskite solar cells. Nano Lett. **19**, 5176 (2019). https://doi.org/10.1021/acs.nanolett.9b01553

[S16] D. Bai, H. Bian, Z. Jin, H. Wang, L. Meng et al., Temperature-assisted crystallization for inorganic $CsPbI_2Br$ perovskite solar cells to attain high stabilized efficiency 14.81%. Nano Energy **52**, 408 (2018). https://doi.org/10.1016/j.nanoen.2018.08.012

[S17] L. Yan, Q. Xue, M. Liu, Z. Zhu, J. Tian et al., Interface engineering for all-inorganic $CsPbI_2Br$ perovskite solar cells with efficiency over 14%. Adv. Mater. **30**, e1802509 (2018). https://doi.org/10.1002/adma.201802509

[S18] W. Chen, H. Chen, G. Xu, R. Xue, S. Wang et al., Precise control of crystal growth for highly efficient $CsPbI_2Br$ perovskite solar cells. Joule **3**, 191 (2019). https://doi.org/10.1016/j.joule.2018.10.011

[S19] J. Tian, Q. Xue, X. Tang, Y. Chen, N. Li et al., Dual interfacial design for efficient $CsPbI_2Br$ perovskite solar cells with improved photostability. Adv. Mater. **31**, e1901152 (2019). https://doi.org/10.1002/adma.201901152

[S20] H. Zhao, Y. Han, Z. Xu, C. Duan, S. Yang et al., A novel anion doping for stable $CsPbI_2Br$ perovskite solar cells with an efficiency of 15.56% and an open circuit voltage of 1.30 V. Adv. Energy Mater. **9**, 1902279 (2019). https://doi.org/10.1002/aenm.201902279

[S21] W. Xu, F. He, M. Zhang, P. Nie, S. Zhang et al., Minimizing voltage loss in efficient all-inorganic $CsPbI_2Br$ perovskite solar cells through energy level alignment. ACS Energy Lett. **4**, 2491 (2019). https://doi.org/10.1021/acsenergylett.9b01662

[S22] Q. Xiao, J. Tian, Q. Xue, J. Wang, B. Xiong et al., Dopant-free squaraine-based polymeric hole-transporting materials with comprehensive passivation effects for efficient all-inorganic perovskite solar cells. Angew. Chem. Int. Ed. **58**, 17724 (2019). https://doi.org/10.1002/anie.201907331

[S23] Y. Zhang, C. Wu, D. Wang, Z. Zhang, X. Qi et al., High efficiency (16.37%) of cesium bromide—passivated all‐inorganic $CsPbI_2Br$ perovskite solar cells. Solar RRL **3**, 1900254 (2019). https://doi.org/10.1002/solr.201900254

[S24] Y. Fan, J. Fang, X. Chang, M.-C. Tang, D. Barrit et al., Scalable ambient fabrication of high-performance $CsPbI_2Br$ solar cells. Joule **3**, 2485 (2019). https://doi.org/10.1016/j.joule.2019.07.015

[S25] W. Xiang, Z. Wang, D. J. Kubicki, W. Tress, J. Luo et al., Europium-doped $CsPbI_2Br$ for stable and highly efficient inorganic perovskite solar cells. Joule **3**, 205 (2019). https://doi.org/10.1016/j.joule.2018.10.008

[S26] J. Zhang, Z. Jin, L. Liang, H. Wang, D. Bai et al., Iodine-optimized interface

for inorganic $CsPbI_2Br$ perovskite solar cell to attain high stabilized efficiency exceeding 14%. Adv. Sci. **5**, 1801123 (2018). https://doi.org/10.1002/advs.201801123

[S27] E.C. Shen, J.D. Chen, Y. Tian, Y. X. Luo, Y. Shen et al., Interfacial energy level tuning for efficient and thermostable $CsPbI_2Br$ perovskite solar cells. Adv. Sci. **7**, 1901952 (2019). https://doi.org/10.1002/advs.201901952

[S28] S.C. Liu, Z. Li, Y. Yang, X. Wang, Y.X. Chen et al., Investigation of oxygen passivation for high-performance all-inorganic perovskite solar cells. J. Am. Chem. Soc. **141**, 18075 (2019). https://doi.org/10.1021/jacs.9b07182

[S29] J. Xue, R. Wang, K.L. Wang, Z.K. Wang, I. Yavuz et al., Crystalline liquid-like behavior: surface-induced secondary grain growth of photovoltaic perovskite thin film. J. Am. Chem. Soc. **141**, 13948 (2019). https://doi.org/10.1021/jacs.9b06940

[S30] S. Fu, W. Zhang, X. Li, L. Wan, Y. Wu et al., Dual-protection strategy for high-efficiency and stable $CsPbI_2Br$ inorganic perovskite solar cells. ACS Energy Lett. **5**, 676 (2020). https://doi.org/10.1021/acsenergylett.9b02716

[S31] Y. Han, H. Zhao, C. Duan, S. Yang, Z. Yang et al., Controlled n−Doping in Air-Stable $CsPbI_2Br$ Perovskite Solar Cells with a Record Efficiency of 16.79%. Adv. Funct. Mater. **30**, 1909972 (2020). https://doi.org/10.1002/adfm.201909972

[S32] H. Zhang, X. Fu, Y. Tang, H. Wang, C. Zhang et al., Phase segregation due to ion migration in all-inorganic mixed-halide perovskite nanocrystals. Nat. Commun. **10**, 1088 (2019). https://doi.org/10.1038/s41467-019-09047-7